

Universal Low-Temperature MWCNT-COOH-Based Counter Electrode and a New Thiolate/Disulfide Electrolyte System for Dye-Sensitized Solar Cells

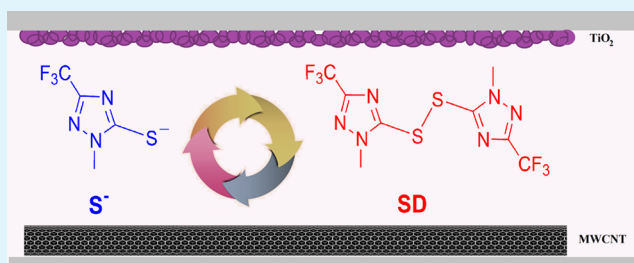
Abdulla Hilmi,[†] Tharallah A. Shoker,[†] and Tarek H. Ghaddar^{*,†}

[†]American University of Beirut, Beirut, Lebanon

Supporting Information

ABSTRACT: A new thiolate/disulfide organic-based electrolyte system composed of the tetrabutylammonium salt of 2-methyl-5-trifluoromethyl-2H-[1,2,4]triazole-3-thiol (S^-) and its oxidized form 3,3'-dithiobis(2-methyl-5-trifluoromethyl-2H-[1,2,4]triazole) (DS) has been formulated and used in dye-sensitized solar cells (DSSCs). The electrocatalytic activity of different counter electrodes (CEs) has been evaluated by means of measuring $J-V$ curves, cyclic voltammetry, Tafel plots, and electrochemical impedance spectroscopy. A stable and low-temperature CE based on acid-functionalized multiwalled carbon nanotubes (MWCNT-COOH) was investigated with our S^-/DS , I^-/I_3^- , T^-/T_2 , and $Co^{II/III}$ -based electrolyte systems. The proposed CE showed superb electrocatalytic activity toward the regeneration of the different electrolytes. In addition, good stability of solar cell devices based on the reported electrolyte and CE was shown.

KEYWORDS: impedance spectroscopy, DSSC, multiwalled carbon nanotubes, thiolate/disulfide electrolyte



INTRODUCTION

In the early 1990s, O'Regan and Grätzel introduced the famous dye-sensitized solar cell (DSSC), and since then it has attracted lots of interest in the scientific community.¹ The high interest in the DSSC research area is mainly due to the DSSC's high efficiency and its low cost of fabrication. Recently, DSSC's efficiencies of 12.3% have been attained using a zinc-porphyrin complex as a sensitizer along with a liquid electrolyte system,² and efficiencies of 15% for perovskite-based solid state DSSC's.³ The former is an optimized DSSC that incorporates a cobalt (II/III)-based redox couple with a thin film of platinum as the counter electrode.

The mostly used redox shuttle in a DSSC is the paradigm iodide-triiodide (I^-/I_3^-) based electrolyte system.^{4,5} However, many research groups have looked for alternative redox couples because of the corrosive behavior of (I^-/I_3^-) toward silver metal that is usually used as electrical contacts in assembled cells, its volatile nature that negatively affects the DSSCs long-term stability, and its high light absorption in the visible region, which would decrease the overall cell's efficiency. In order to overcome the above-mentioned drawbacks, various inorganic and organic-based redox couples^{6–20} besides (I^-/I_3^-) have been introduced by different groups as alternative redox electrolytes. Recently, great interest in the organic-based thiolate/disulfide redox couple has emerged.^{21–31} The attracting features of the thiolate/disulfide redox couples reside in their low light absorption and retarded electron recombination processes,⁹ where both of these features have positive effects on the total DSSC's efficiency. In addition, some

thiolate/disulfide redox couples have been successfully used in the promising quantum-dots based and p-type solar cells.^{32–34}

One of the best cathode catalyst that is used in high-efficiency DSSCs is Pt due to its excellent conductivity and high catalytic activity toward the (I^-/I_3^-) electrolyte regeneration. However, the use of Pt in DSSCs has some disadvantages, particularly, its high cost and limited availability,³⁵ which is a major drawback in the mass production of DSSCs. In addition, a recent study shows that Pt could be unstable with the (I^-/I_3^-) electrolyte during prolonged stability tests.³⁶ Another drawback of Pt as a cathode material in a DSSC is the use of high temperatures ($\sim 400^\circ\text{C}$) during its preparation which renders its use in flexible type DSSCs difficult. Moreover, Pt shows poor electrocatalytic activity with most thiolate/disulfide redox couples, which motivated researchers to investigate various materials to be used as cathodes in a DSSC, such as metal carbides,³⁷ metal phosphides,³⁸ CoS ,^{39,40} NiS ,⁴¹ PEDOT,^{39,40} carbonaceous material,^{28,42–44} and carbon nanotubes.^{22,45–47} The poor catalytic activity of Pt toward the thiolate/disulfide redox couples could be due to the adsorption of the sulfur atoms onto Pt which in turn slows down the catalytic reduction of the oxidized disulfide species.³⁷ Therefore, it is imperative to seek Pt-free cathodic material to be used in DSSCs that show high electrocatalytic activity toward the commonly used redox

Received: March 14, 2014

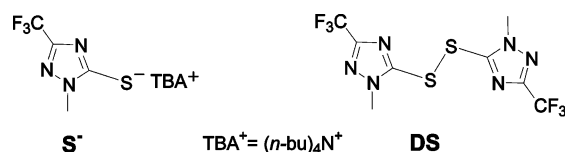
Accepted: May 12, 2014

Published: May 12, 2014

shuttles, possess good long-term stability, prepared at low temperatures for the flexible-type DSSCs and of low cost.

In this work, we report on a new organic-based thiolate/disulfide electrolyte system composed of the tetrabutylammonium salt of 2-methyl-5-trifluoromethyl-2*H*-[1,2,4]triazole-3-thiol (S^-) and its oxidized form 3,3'-dithiobis(2-methyl-5-trifluoromethyl-2*H*-[1,2,4]triazole) (DS) (Scheme 1 and

Scheme 1. Structures of the Organic Electrolyte Components, Tetrabutylammonium Salt of 2-Methyl-5-trifluoromethyl-2*H*-[1,2,4]triazole-3-thiol (S^-) and 3,3'-Dithiobis(2-methyl-5-trifluoromethyl-2*H*-[1,2,4]triazole) (DS)



Scheme S2 in the Supporting Information), and on the use of Pt-free cathode material based on acid-functionalized multiwalled carbon nanotubes (MWCNT-COOH), that can be used efficiently with the above-mentioned electrolyte system in addition to Co(II/III), (I^-/I_3^-) and another conventional thiolate/disulfide electrolyte system based on 5-mercapto-1-methyltetrazole tetramethylammonium salt/di-5-(1-methyltetrazole) disulfide (T^-/T_2)²⁴ (see the Supporting Information, Scheme S1).

EXPERIMENTAL SECTION

Materials and Instrumentation. All chemicals were purchased from Sigma-Aldrich and used as supplied. The N719 and D35 dyes were purchased from Solaronix (Switzerland), and Dyenamo (Sweden), respectively. 5-Mercapto-1-methyltetrazole tetramethylammonium salt/di-5-(1-methyltetrazole) disulfide thiolate/disulfide (T^-/T_2), Co^{II}(2,2'-bipyridine)₃·3PF₆, and Co^{III}(2,2'-bipyridine)₃·3PF₆ were synthesized according to procedures found in the literature.^{24,48} FTO glass "Tec15" was purchased from Pilkington (USA). TiO₂ colloids were purchased from Dyesol (Australia). The MWCNT-COOH (20–30 nm outer-diameter and with 1.2 wt % COOH groups) were purchased from Cheap Tubes (USA), and acetylene black was purchased from Strem Chemicals (USA). The NMR spectra (¹H and ¹³C) were measured on a Bruker AM 300 MHz spectrometer. The electrochemical setup for cyclic voltammetry in nonaqueous solution consisted of a three-electrode cell, with a glassy carbon electrode or the respective CE as the working electrode, a Pt wire ~1 mm diameter as the counter electrode, and Ag/Ag⁺ (10 mM AgNO₃) as the reference electrode. All solution-phase electrochemical measurements were made in 0.1 M tetrabutylammonium hexafluorophosphate or lithium perchlorate in acetonitrile, and Fc/Fc⁺ standard (0.63 vs NHE in acetonitrile) was used as a reference. Electrochemical impedance spectra (EIS) of the DSSCs were performed with a CH Instruments 760B potentiostat (USA). The obtained impedance spectra were fitted with the Z-view software (v2.8b, Scribner Associates Inc.). For the DSSC's studied, the EIS spectra were performed at open-circuit voltages (at various white light intensities) in the frequency range 0.1 Hz to 1 × 10⁵ Hz with oscillation potential amplitudes of 10 mV at RT, whereas for the dummy cells, the EIS experiments were performed at an applied potential of 0 V under dark conditions. Photocurrent vs voltage characteristics were measured with a Keithley 2400 sourcemeter. The cell dimensions were 1 × 1 cm and the irradiated area of the cell was 0.126 cm². The SEM images of the MWCNT-COOH based electrodes were taken with Tescan Vega 3.

Counter Electrodes (CEs) Preparation. The Pt counter electrodes were fabricated by applying a 2–3 μL/cm² of 5 mM H₂PtCl₆ in 2-propanol to the FTO glass, followed by heating in an

oven at 400 °C for 20 min. The MWCNT-COOH based CEs were fabricated by the doctor blading method (3 layers of 3 M tape) using a CNT paste that was prepared as follows: a mass ratio of 1:1:8:80 of acetylene black:poly vinylidene difluoride (PVDF):MWCNT-COOH:*N*-methyl-2-pyrrolidone (NMP) was ultrasonicated with a sonicator horn for 10 min. Finally, the electrode was dried at 120 °C in air overnight. This afforded the CNT-based CEs with thicknesses of ~10 μm films.

Solar Cell Fabrication. Dye-sensitized solar cells were fabricated using standard procedures. The TiO₂ films were made from colloidal solutions using the doctor blading method (2× times) and then heated to 480 °C for 30 min. This afforded a 12 μm thick TiO₂ film, on top of which a 4 μm TiO₂ scattering layer (300 nm TiO₂ particles) was deposited and reheated at 480 °C for 30 min. A TiCl₄ post-treatment was applied to the films following reported procedures in the literature.⁴⁹ These films were then reheated at 480 °C for 30 min. The TiO₂ films were stained by the respective dye solution (0.3 mM) in 1:1 acetonitrile:*t*-butyl alcohol for 18 h. Cells assemblies were formed by sealing the counter electrodes to the TiO₂ electrode with a 60 μm Surlyn (Dupont) spacer at ~100 °C for 3 min. The corresponding electrolyte was introduced through two small holes, previously drilled through the counter electrode, which were then sealed with Surlyn. The optimized thiolate/disulfide electrolyte (EL1) used was as follows; 0.4 M (S^-), 0.15 M (DS), 0.5 M *tert*-butylpyridine (TBP), and 0.05 M lithium bis(trifluoromethanesulfonyl)imide (LiTFSI) in acetonitrile. The (I^-/I_3^-) electrolyte (EL2) contained 1.0 M 1,3-dimethylimidazolium iodide (DMII), 0.1 M guanadimium thiocyanate (GuNCS), 0.05 M LiI, 0.03 M I₂, and 0.5 M TBP in acetonitrile, the Co(II/III) electrolyte (EL3) was composed of 0.2 M Co^{II}(2,2'-bipyridine)₃·2PF₆, 0.05 M Co^{III}(2,2'-bipyridine)₃·3PF₆, 0.05 M LiClO₄, and 0.25 M TBP in acetonitrile, whereas the T^-/T_2 (EL4) was composed of 0.4 M (T^-), 0.4 M (T_2), 0.5 M TBP, and 0.05 M LiTFSI in 6:4 acetonitrile:ethylenecarbonate.

Preparation of 2-Methyl-5-trifluoromethyl-2*H*-[1,2,4]triazole-3-thiol, (SH). To a stirring solution of 2-methylthiosemicarbazide (1.0 g, 9.5 mmol) in xylene (150 mL) was added trifluoroacetic acid (1.3 g, 11.4 mmol) and the solution was refluxed using a Dean–Stark apparatus until no water was produced (~1–2 h). The volatiles were taken off under reduced pressure, and the product was dissolved in ethyl acetate (200 mL) and washed with 2 M HCl(aq), dried over anhydrous MgSO₄, and then the solvent was taken off under reduced pressure. This afforded the desired product as a pure white solid (1.5 g, 86%). ¹H NMR (CDCl₃, 300 MHz), δ (ppm): 3.84 (s, 3H), 13.64 (br s, 1H). ¹³C NMR (CDCl₃, 75 MHz), δ (ppm): 36.44, 116.68 (q), 139.91 (q), 166.74. MS (ESI): *m/z* = 181.8 [M–H⁺][–] calcd for C₄H₃F₃N₃S, 182.2.

Preparation of 2-Methyl-5-trifluoromethyl-2*H*-[1,2,4]triazole-3-thiolate Tetrabutylammonium Salt, (S^-). To a methanolic solution of SH was added 1 eq. of tetrabutylammonium hydroxide (1 M in MeOH) and stirred for 1 h under a N₂ atmosphere. The solvent was taken off under reduced pressure, and the afforded oil was dried at 60 °C under vacuum overnight. This afforded the salt as an off-white solid in quantitative yield. ¹H NMR (CDCl₃, 300 MHz), δ (ppm): 0.95 (t, 12H), 1.40 (m, 8H), 1.75 (m, 8H), 3.40 (m, 8H), 3.83 (s, 3H), 3.84 (s, 3H), 13.64 (br s, 1H). MS (ESI): *m/z* = 181.8 [M–TBA⁺][–] calcd for C₄H₃F₃N₃S, 182.2.

Preparation of 3,3'-Dithiobis(2-methyl-5-trifluoromethyl-2*H*-[1,2,4]triazole), (DS). To a solution of SH (1.0 g, 5.0 mmol) in 100 mL of 1:1 THF:water was added K₂CO₃ (0.69 g, 5.0 mmol). While under stirring, iodine (0.64 g, 2.5 mmol) in 20 mL of THF was added dropwise. After the mixture was stirred at room temperature for 20 min, the volatiles were taken off under a vacuum and the residue was extracted with CH₂Cl₂ and dried over MgSO₄ and the solvent was removed under reduced pressure. The crude product was purified on a silica gel column using 1% ethyl acetate in hexane. This afforded the disulfide product as a white pure solid (0.35 g, 35% yield). ¹H NMR (CDCl₃, 300 MHz), δ (ppm): 4.03 (s). ¹³C NMR (CDCl₃, 75 MHz), δ (ppm): 37.70, 118.05 (q), 152.05 (q), 154.79. MS (ESI): *m/z* = 365.2 [M+H⁺]⁺ calcd for C₈H₇F₆N₆S₂, 365.3.

RESULTS AND DISCUSSION

The S^-/DS redox couple was designed in a way to have good solubility in various solvents and with the right redox potential to ensure an efficient regeneration of the oxidized dye upon electron injection. This was accomplished by the introduction of a trifluoromethyl group on the mercapto-triazole ring which in turn affected positively the solubility of the reduced salt (S^-) and oxidized forms (DS) in various solvents including the somehow nonpolar solvents dichloromethane and chloroform. The redox potential of S^-/DS was measured to be $E_{1/2} = 0.50$ V against NHE in acetonitrile (see the Supporting Information, Figure S1), which is similar to that of iodide/triiodide in organic solvents.⁵⁰ Such a redox potential would make S^-/DS possess the desirable thermodynamic driving force to efficiently regenerate the most commonly used dye, N719, in a DSSC ($-\Delta G \approx 0.6$ eV).

To start, we constructed various DSSCs and evaluated their photovoltaic parameters while using S^-/DS as the electrolyte with various concentration ratios of S^- and DS, Pt/FTO as the counter electrode and N719 as the dye of choice. The optimized S^-/DS electrolyte composition (EL1), that was further investigated using different CEs, was as follows: 0.4 M S^- , 0.15 M DS, 0.5 M TBP and 0.05 M LiTFSI in acetonitrile. As a reference, cells with an iodine-based electrolyte EL2 (1.0 M DMII, 0.1 M GuNCS, 0.05 M LiI, 0.03 M I_2 and 0.5 M TBP in acetonitrile) and Pt as a counter electrodes were also fabricated. Figure 1 depicts the photocurrent density–voltage

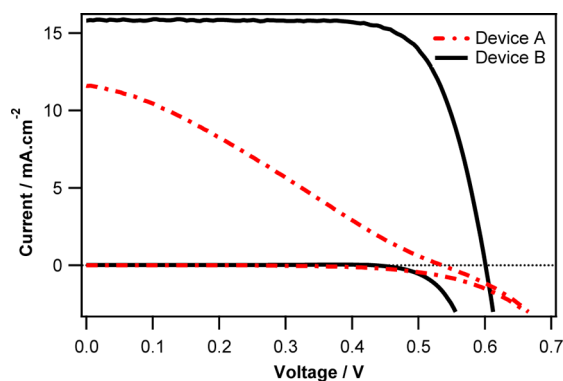


Figure 1. Photocurrent–voltage (J – V) curves of device A with Pt CE and EL1 (dotted-dashed-red) and device B with Pt CE and EL2 (solid-black). Measured under 100 mW cm^{-2} simulated AM1.5 spectrum with an active area = 0.126 cm^2 .

(J – V) curves of devices A (N719/EL1/Pt) and B (N719/EL2/Pt) under air mass 1.5 global (AM 1.5 G) (100 mW/cm^2) irradiation. The detailed photovoltaic parameters, that are the open-circuit voltage (V_{oc}), fill factor (FF), short-circuit current density (J_{sc}) and photovoltaic conversion efficiency (η) are given in Table 1. As can be seen, device A showed much lower efficiency than device B ($\eta = 2.62$ and 7.21% , respectively) and strikingly lower fill factor (FF = 0.42 for device A and 0.75 for device B).

It is well-known that the internal resistance in a DSSC affects dramatically the fill factor which in turn governs the overall efficiency. Electrochemical Impedance Spectroscopy (EIS) is one of the powerful tools that can be used to explore the electrochemical processes in a DSSC while utilizing the appropriate transmission line model.^{51–53} Upon performing EIS experiments on symmetrical dummy cells (i.e., CE//

Table 1. Photovoltaic Performance of Devices A to H

device	counter electrode	electrolyte	J_{sc} (mA cm^{-2})	V_{oc} (mV)	FF	η (%) ^e
A	Pt	EL1 ^a	11.6	534	0.42	2.62
B	Pt	EL2 ^b	15.8	602	0.75	7.21
C	MWCNT-COOH	EL1	15.4	580	0.58	5.20
D	MWCNT-COOH	EL2	15.6	611	0.68	6.51
E	MWCNT-COOH	EL3 ^c	6.7	835	0.66	3.72
F	Pt	EL3	6.3	852	0.66	3.53
G	MWCNT-COOH	EL4 ^d	11.6	547	0.61	4.07
H	Pt	EL4	11.7	557	0.61	3.95

^aElectrolyte (EL1); 0.4 M (S^-), 0.15 M (DS), 0.5 M TBP, and 0.05 M LiTFSI in acetonitrile. ^bElectrolyte (EL2); 1.0 M DMII, 0.1 M GuNCS, 0.05 M LiI, 0.03 M I_2 , and 0.5 M TBP in acetonitrile. ^cElectrolyte (EL3); 0.2 M $\text{Co}^{\text{II}}(2,2'$ -bipyridine)₃·2PF₆, 0.05 M $\text{Co}^{\text{III}}(2,2'$ -bipyridine)₃·3PF₆, 0.05 M LiClO₄, and 0.25 M TBP in acetonitrile. ^dElectrolyte (EL4); 0.4 M (T^-), 0.4 M (T_2), 0.5 M TBP, and 0.05 M LiTFSI in 6:4 acetonitrile:ethylenecarbonate. ^eMeasured under 100 mW cm^{-2} simulated AM1.5 spectrum with an active area = 0.126 cm^2 .

electrolyte//CE), the series resistance (R_s), charge transfer resistance (R_{CT}) and double layer capacitance (C_μ) at the CE/electrolyte interface, in addition to the diffusion impedance (Z_N) of the redox couple can be evaluated. Typical EIS of dummy cells incorporating EL1 (device A') and EL2 (device B') with Pt as the CE are shown in Figure 2 as Nyquist and Bode plots. The transmission line model we used for dummy cells with Pt CE's is the traditional equivalent circuit for a

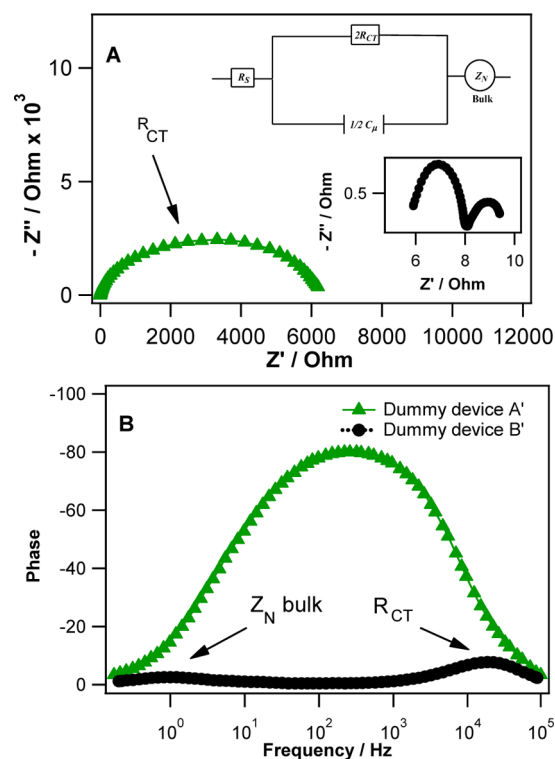


Figure 2. (A) Impedance spectra of the dummy device A' (solid-triangle-green) and (inset) device B' (solid-circle-black) as Nyquist plots and (B) as Bode plots.

Table 2. Impedance Parameters of the Dummy Devices A' to H'

device ^a	electrode	electrolyte	R_{CT} (Ω cm ²)	C_{μ} (μ F cm ⁻²)	R_s (Ω)
A'	Pt	EL1	2960 ± 2	15 ± 1	6.0 ± 0.1
B'	Pt	EL2	1.0 ± 0.1	25 ± 2	6.0 ± 0.1
C'	MWCNT-COOH	EL1	0.5 ± 0.1	18 ± 3	7.2 ± 0.1
D'	MWCNT-COOH	EL2	0.5 ± 0.1	18 ± 3	7.2 ± 0.1
E'	MWCNT-COOH	EL3	0.3 ± 0.1	22 ± 1	7.2 ± 0.1
F'	Pt	EL3	18.2 ± 1.0	20 ± 1	6.4 ± 0.1
G'	MWCNT-COOH	EL4	<0.2	-	6.2 ± 0.1
H'	Pt	EL4	75 ± 1	20 ± 1	6.0 ± 0.1

^aMeasured under dark conditions with an applied potential = 0 V and a cell area = 1 × 1 cm².

sandwich cell configuration detailed by Hauch and Georg,⁵⁴ Figure 2A. Accordingly, R_s was evaluated from the onset of the first semicircle at ~100 kHz, whereas R_{CT} and C_{μ} were evaluated from the first semicircle between ~100 and 0.1 kHz. As can be seen, the Pt CE shows a large R_{CT} = 2960 Ω cm² value with EL1 (C_{μ} = 1.5 × 10⁻⁵ F cm⁻²), whereas that with the EL2-based dummy cell the value is much smaller (R_{CT} = 1 Ω cm² and C_{μ} = 2.5 × 10⁻⁵ F cm⁻²), Table 2. Both dummy cells showed similar R_s values as expected (R_s ≈ 6 Ω). Such higher R_{CT} for device A' at the CE/electrolyte interface is thought to be the reason behind the measured lower FF, thus lower efficiency when compared to device B.

Therefore, it seems that platinum is a less efficient catalyst for the reduction of DS and thus regeneration of the S⁻/DS electrolyte system in our DSSCs. Such a result drove us to investigate the use of other CE material in combination with EL1, such as CoS, NiS, PEDOT, graphite, and multiwalled carbon nanotubes (MWCNT) (see the Supporting Information, Figure S2). Surprisingly, none of these commonly used materials with other thiolate based electrolytes worked well with our EL1 system, except for the latter, MWCNT. Generally speaking, the methods by which MWCNT-based electrodes are fabricated as CEs for DSSCs involve either transferring the as grown MWCNTs onto FTO,^{22,46,55-58} or applying a solution of MWCNTs onto FTO by spincoating⁵⁹ or spraying.^{60,61} However, these different methods result in weakly adherent MWCNT films on FTO. In order to enhance adhesion, different research groups apply the MWCNTs as a paste that contains a binder followed by a sintering process at high temperatures (more than 300 °C).⁶²⁻⁶⁵ We started by optimizing an MWCNT paste that could be easily used to fabricate reproducible films with good adherence to FTO and avoiding the use of high temperatures. The latter characteristic is of high importance to the DSSC industry especially for the production of flexible-type DSSCs', such as in the case of polyethylene naphthalate (PEN) or polyethylene terephthalate (PET) based electrodes.^{45,66} The optimized paste consisted of acetylene black, PVDF, MWCNT-COOH in NMP with a mass ratio of 1:1:8:80. Films that were made using 3 layers of scotch tape by the doctor blading method afforded ~10 μ m films of adherent and good-quality films. The reason behind choosing acid-functionalized carbon nanotubes was because of their good dispersion in NMP, unlike the unfunctionalized material. Figure 3 shows a digital photo of the MWCNT-COOH film on FTO and its SEM image. As can be seen from the SEM image, the microstructure of the MWCNT-COOH-based CE reveals that the film has a porous and uniform structure composed of randomly cross-stacked nanotubes.

Figure 4 shows the J - V curves of devices C (N719/EL1/MWCNT-COOH) and D (N719/EL2/MWCNT-COOH),

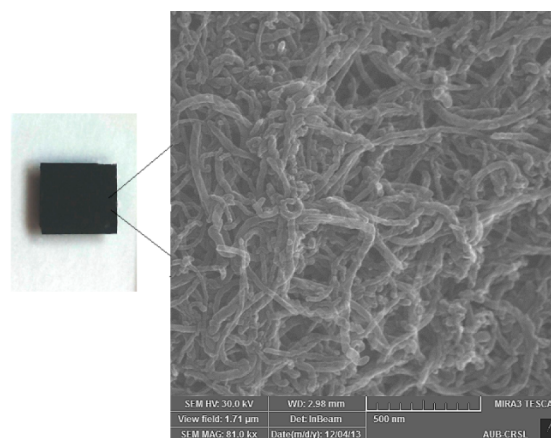


Figure 3. Digital photo of the MWCNT-COOH based film on FTO and the scanning electron microscopy (SEM) image.

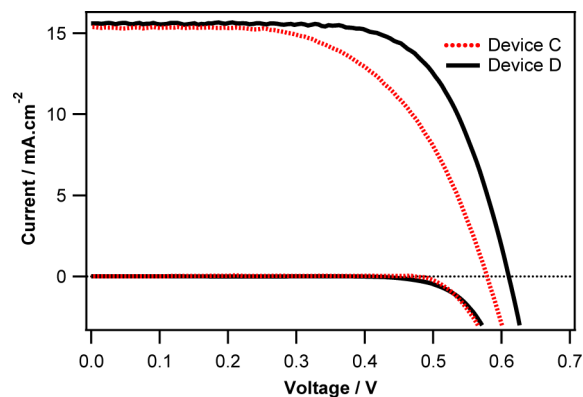


Figure 4. Photocurrent–voltage (J - V) curves of device C with MWCNT-COOH CE and EL1 (dotted-red) and device D with MWCNT-COOH CE and EL2 (solid-black). Measured under 100 mW cm⁻² simulated AM1.5 spectrum with an active area = 0.126 cm².

where the photovoltaic parameters were measured to be V_{oc} = 580 and 611 mV, J_{sc} = 15.4 and 15.6 mA cm⁻², FF = 0.58 and 0.68, and η = 5.20 and 6.51%, respectively, Table 1. To understand the differences in the photovoltaic parameters between devices C and D, we performed EIS measurements on the two assembled cells (devices C and D) at V_{oc} under different light intensities. EIS spectra were analyzed using an established equivalent-circuit that interprets the different interfaces in a functional DSSC through a transmission line model.^{67,68} Figure 5 shows a plot of the chemical capacitance (C_{μ}) and the charge recombination resistance (R_{CT}) values at the TiO₂/electrolyte interface for the two cells extracted from the EIS experiments versus the applied voltage ($\mu E_F - E_{F,redox}$),

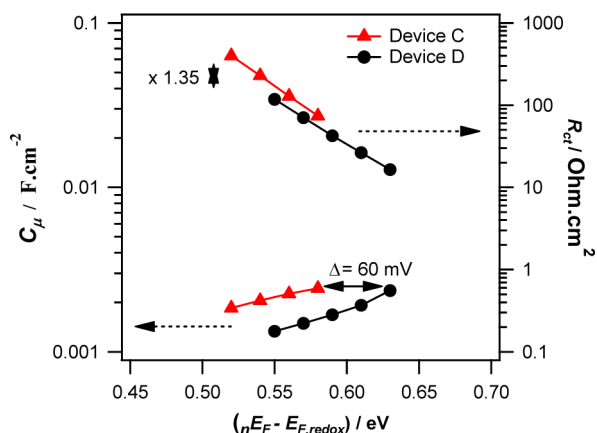


Figure 5. Capacitance and charge transfer resistance values obtained from EIS for devices C (solid-triangle-red) and D (solid-circle-black).

where nE_F is the electron quasi-Fermi energy level in the TiO_2 film and $E_{F,\text{redox}}$ is the electrolyte redox Fermi level. The C_μ values for the two cells show an exponential behavior as a function of the applied voltage, where this is due to the trap energy distribution below the conduction band edge.⁶⁹ A shift in the $(nE_F - E_{F,\text{redox}})$ toward higher or lower values could be attributed to an upward or downward shifts in the conduction band edge with respect to the electrolyte Fermi level, respectively.^{70,71} Device C shows a shift $\Delta(nE_F - E_{F,\text{redox}})$ of ~ 60 mV lower than device D. Therefore, the lower V_{oc} of device C is most probably caused by the electrolyte EL1 downward shifting the TiO_2 CB by more than 180 mV when compared to the device D, and this is countered back by a more positive $E_{F,\text{redox}}$ for EL1 by ~ 150 mV, which causes a lower V_{oc} by ~ 31 mV. In addition, the electron lifetime (τ_n) in devices C and D were evaluated from the EIS experiments ($\tau_n = R_{\text{ct}}C_\mu$) and are shown in Figure S3 in the Supporting Information, and are consistent with the slower recombination processes in device C when compared to D.

The EIS spectra of dummy cells incorporating EL1 (device C') and EL2 (device D') with MWCNT-COOH as both CEs are shown in Figure 6. As can be seen, both dummy cells showed similar $R_{\text{CT}} = 0.5 \Omega \text{ cm}^2$, $C_\mu = 1.8 \times 10^{-5} \text{ F cm}^{-2}$, and $R_S = 7.2 \Omega$ values, Table 2. The relatively small value of R_{CT} in both cells suggests that the MWCNT-COOH CE is a good electroactive material for both electrolytes. However, to evaluate the reaction kinetics at the Pt and MWCNT-COOH

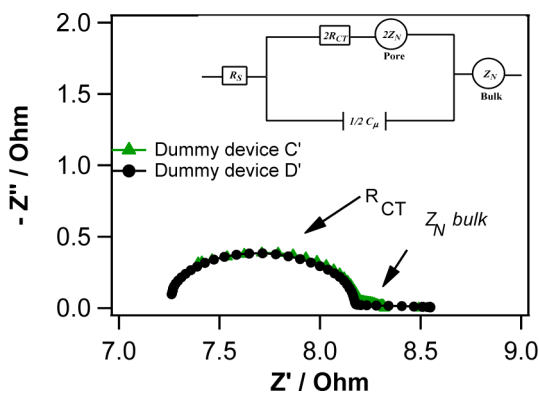


Figure 6. Impedance spectra of the dummy device C' (solid-triangle-red) and device D' (solid-circle-black) as Nyquist plots.

counter electrodes, we performed Tafel polarization measurements of the four dummy cells mentioned above (devices A', B', C', and D'), Figure 7. Devices B', C', and D' exhibited large

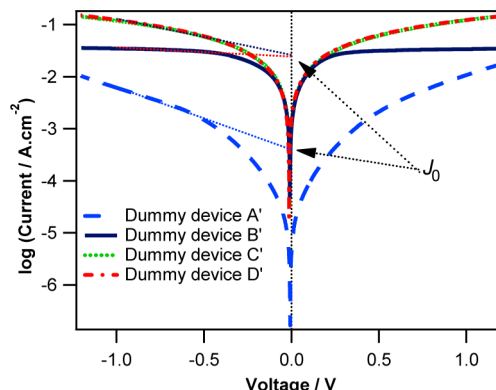


Figure 7. Tafel plots of dummy devices A' (dashed-blue), B' (solid-black), C' (dotted-green), and D' (dotted-dashed-red).

exchange current densities ($J_0 = 24.2$ for device B' and 26.0 mA cm^{-2} for devices C' and D') in comparison with device A' ($J_0 = 0.4 \text{ mA cm}^{-2}$).

The value of J_0 is the kinetic component directly correlated with the electrochemical reaction rate constant and inversely proportional to R_{CT} , as described in eq 1.

$$J_0 = \frac{RT}{nFR_{\text{CT}}} \quad (1)$$

where R is the gas constant, T is the absolute temperature, n is the number of electrons associated with reaction, and F is the Faraday constant. The calculated R_{CT} using eq 1 for devices C' and D' was $0.5 \Omega \text{ cm}^2$, which is of similar value as the one extracted from the EIS experiments. However, since devices C' and D' incorporate a porous CE unlike devices A' and B', it is difficult to discern whether the small R_{CT} (measured from EIS or calculated from the Tafel plots) is due to the intrinsically higher catalytic activity and/or from the higher surface area of the MWCNT-COOH based CE. Therefore, to distinguish between specific catalytic activity and surface area effects, we performed cyclic voltammetry using Pt and MWCNT-COOH films on FTO with 1 mM I_3^- , 10 mM I^- , and 0.1 M LiClO_4 in acetonitrile, Figure 8. For the I^-/I_3^- redox couple on both the MWCNT-COOH and Pt electrodes the obtained CV curves were similar with two pairs of redox peaks, where the pair present at the relatively more negative potentials is attributed to the oxidation/reduction of I^-/I_3^- at the electrode surface.⁷² And since the standard electrochemical rate constant of a redox system is negatively correlated with the peak-to-peak separation (ΔE_p),⁷³ we concluded that the MWCNT-COOH based electrode has a slightly lower performance than Pt toward the I^-/I_3^- redox reaction (ΔE_p values of 0.53 and 0.56 V for Pt and MWCNT-COOH, respectively). A more profound difference between the two electrodes was seen with EL1, Figure 9, where the ΔE_p values were found to be 1.88 and 0.97 V for Pt and MWCNT-COOH, respectively, and are consistent with the Tafel and EIS measurements of devices A' and C'. These results explain the slightly lower performance of device D ($\eta = 6.51\%$) when compared to device B ($\eta = 7.21\%$) and the superior performance of device C when compared to A. Nevertheless, the good performance of the MWCNT-COOH CE toward EL1 and EL2 is concluded to be due to its high

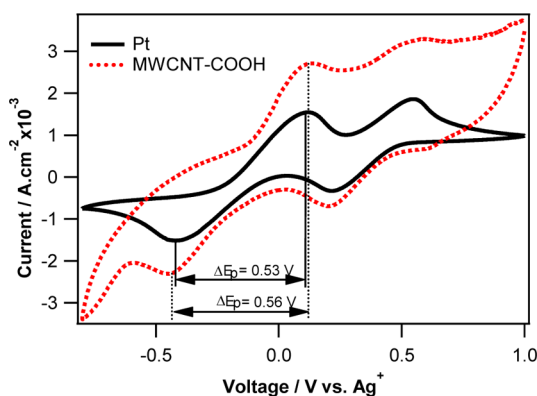


Figure 8. Cyclic voltammograms obtained at a scan rate of 50 mV s^{-1} for the oxidation and reduction of the I^-/I_3^- (1 mM I_3^- , 10 mM I^- , and 0.1 M LiClO_4 in acetonitrile) using Pt on FTO (solid-black) and MWCNT-COOH film on FTO (dotted-red) electrodes.

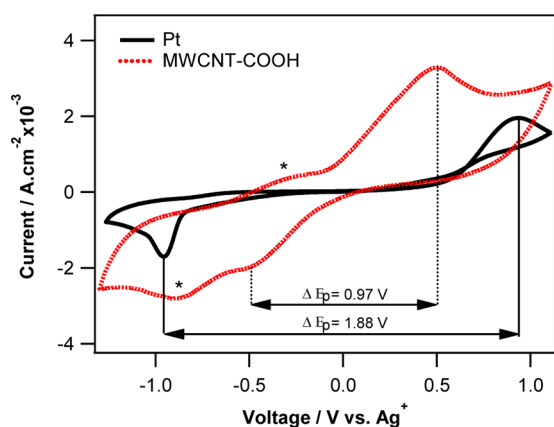


Figure 9. Cyclic voltammograms obtained at a scan rate of 50 mV s^{-1} for the oxidation and reduction of the S^{2-}/DS ($10 \text{ mM}/1 \text{ mM}$ and 0.1 M LiClO_4 in acetonitrile) using Pt on FTO (solid-black) and MWCNT-COOH film on FTO (dotted-red) electrodes (peaks with an asterisk are due to the oxidation/reduction peaks of the carboxylic acid moieties in the MWCNT-COOH film).

electroactive surface area in addition to its intrinsic electrocatalytic activity toward both electrolytes. As for the former characteristic, we believe this is due to the fact that the low temperature processing of the MWCNT-COOH film does not cause significant decarboxylation reactions, where a loss of the oxygen containing groups might influence negatively the electroactivity, since it is believed that these moieties in oxidized MWCNT-COOH are responsible for their electroactivity.⁷⁴ In addition, the C_μ values (between 14 and $22 \mu\text{F cm}^{-2}$) of the MWCNT-COOH film extracted from the EIS experiments performed on the various dummy cells are similar to those obtained for Pt (between 15 to $25 \mu\text{F cm}^{-2}$) and thus suggest similar specific electroactive surface area in both films. Moreover, the J_0 values obtained from the Tafel plots and the R_{CT} values for devices B', C', and D' suggest fast and similar electron transfer reaction rates at both films. Lastly, the similar R_s values measured in all of the dummy cells reflect the good conductivity of the MWCNT-COOH CEs and are comparable with the Pt CEs.

The above-mentioned positive results motivated us to investigate the use of the MWCNT-COOH-based CE with other electrolyte systems, mainly a $\text{Co}(\text{bpy})_3^{\text{II/III}}$ electrolyte system and the thiolate/disulfide (T^-/T_2) electrolyte system as

reported by Wang et al.²⁴ We constructed DSSC devices using the commercially available organic dye (D35, see the Supporting Information, Scheme S3) and an electrolyte system (EL3) composed of $0.20 \text{ M Co}^{\text{II}}(2,2'\text{-bipyridine})_3\cdot 2\text{PF}_6$, $0.05 \text{ M Co}^{\text{III}}(2,2'\text{-bipyridine})_3\cdot 3\text{PF}_6$, 0.05 M LiClO_4 , and 0.25 M TBP in acetonitrile, in addition to devices with the N719 dye and an electrolyte (EL4) composed of 0.4 M T^- , 0.4 M T_2 , 0.05 M LiTFSI , and 0.5 M TBP in $6:4$ acetonitrile:ethylenecarbonate. The four devices were as follows: device E (D35/EL3/MWCNT-COOH), device F (D35/EL3/Pt), device G (N719/EL4/MWCNT-COOH), and device H (N719/EL4/Pt). Figure 10 shows the J - V curves of devices E and F, where

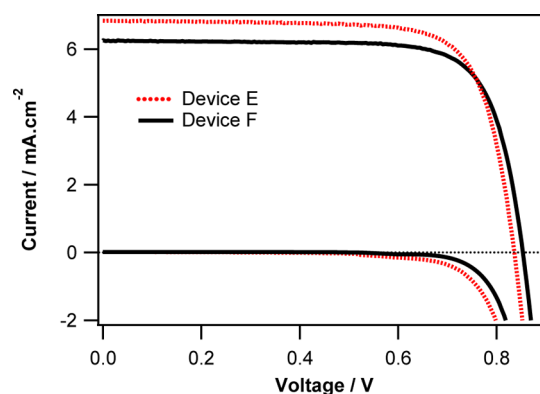


Figure 10. Photocurrent–voltage (J - V) curves of device E with MWCNT-COOH CE and EL3 (dashed-red) and device F with Pt CE and EL3 (solid-black). Measured under 100 mW cm^{-2} simulated AM1.5 spectrum with an active area $= 0.126 \text{ cm}^2$.

the photovoltaic parameters were measured to be $V_{\text{oc}} = 835$ and 852 mV , $J_{\text{sc}} = 6.7$ and 6.3 mA cm^{-2} , $\text{FF} = 0.66$, and $\eta = 3.72$ and 3.53% , respectively, Table 1. The EIS of dummy cells incorporating EL3 (devices E' and F') with MWCNT-COOH and Pt as CE's, respectively, are shown in Figure 11.

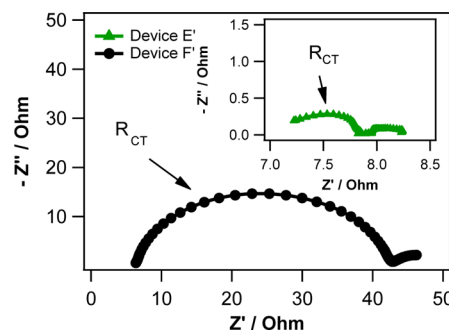


Figure 11. Impedance spectra of the dummy device E' (solid-triangle-green) and (inset) device F' (solid-circle-black) as Nyquist plots.

The calculated impedance values for device E' were $R_{\text{CT}} = 0.3 \Omega \text{ cm}^2$, $C_\mu = 2.2 \times 10^{-5} \text{ F cm}^{-2}$ and $R_s = 7.2 \Omega$, whereas that of device F' were $R_{\text{CT}} = 18.2 \Omega \text{ cm}^2$, $C_\mu = 2.0 \times 10^{-5} \text{ F cm}^{-2}$ and $R_s = 6.4 \Omega$, Table 2. Again, these results show the superior performance of the MWCNT-COOH CE toward the cobalt-based electrolyte (EL3) when compared to the conventional platinum electrode.

As for devices G and H, Figure 12 depicts the J - V curves of the two devices, where the photovoltaic parameters were measured to be $V_{\text{oc}} = 547$ and 557 mV , $J_{\text{sc}} = 11.6$ and 11.7 mA cm^{-2} , $\text{FF} = 0.614$, and 0.606 , and $\eta = 4.07$ and 3.95% ,

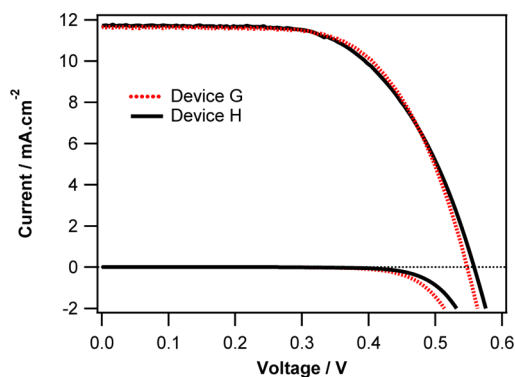


Figure 12. Photocurrent–voltage (J – V) curves of device G with MWCNT-COOH CE and EL4 (dashed-red) and device H with Pt CE and EL4 (solid-black). Measured under 100 mW cm^{-2} simulated AM1.5 spectrum with an active area = 0.126 cm^2 .

respectively, Table 1. The EIS of dummy cells incorporating EL4 (device G' and device H') with MWCNT-COOH and Pt as CE's, respectively, are shown in Figure 13. The calculated

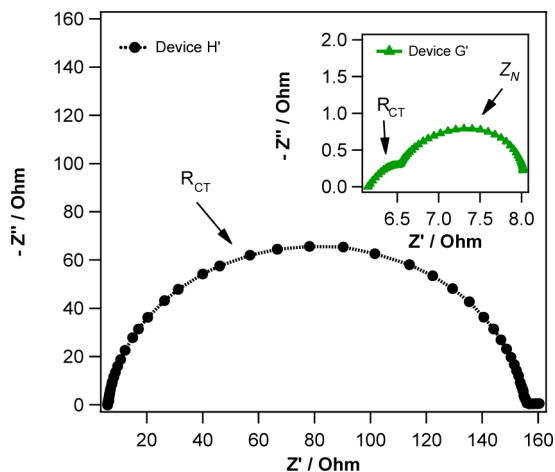


Figure 13. Impedance spectra of the dummy device H' (solid-circle-black) and (inset) device G' (solid-triangle-green) as Nyquist plots.

impedance values for device G' were $R_{CT} < 0.2 \Omega \text{ cm}^2$ and $R_S = 6.2 \Omega$, whereas that of device H' were $R_{CT} = 75 \Omega \text{ cm}^2$, $C_\mu = 2.0 \times 10^{-5} \text{ F cm}^{-2}$, and $R_S = 6.0 \Omega$, Table 2. Interestingly, in the dummy cell G' the Z_N impedance due to the electrolyte diffusion was more obvious than in all of the studied dummy cells. We attribute this to the higher viscosity of the solvent used in EL4 because of introduction of the ethylenecarbonate as a cosolvent. Tafel plots and CV curves of devices E' to H' mirror the results obtained by EIS experiments (see the Supporting Information, Figures S4–S7).

The higher J_{sc} of device E and total efficiency are consistent with the higher electrocatalytic activity of the MWCNT-COOH than the Pt CE toward EL3, and the higher efficiency of device G when compared to H is mainly due to the better FF of the former which is mainly caused by its smaller R_{CT} at the CE/electrolyte interface. However, the reason behind the lower V_{oc} values (by $\sim 17 \text{ mV}$ for device E when compared to device F and by $\sim 10 \text{ mV}$ for device G when compared to device H) and the increase of the corresponding dark currents are not clear at this stage, but might be due to weakly adhered MWCNTs that may detach from the FTO glass substrate and

get deposited on the TiO_2 photoanode side, and thus promoting the dark currents. Similar surprising results have been reported by Kavan et al. for graphene nanoplatelets CE when used with cobalt-based electrolyte system.⁵³

Finally, the J – V curves of a fresh and aged device C stored at ambient light and temperature conditions for more than 2000 h are shown in Figure 14. The efficiency decreased by 13.5% from

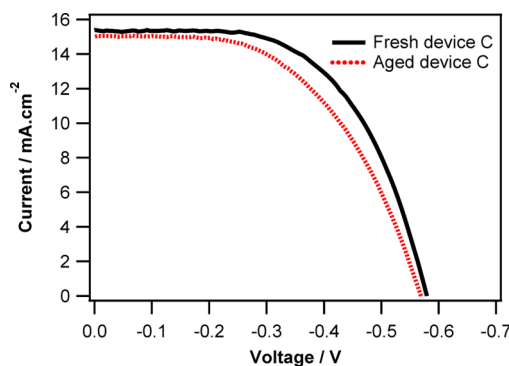


Figure 14. Photocurrent–voltage (J – V) curves of fresh device C (solid-black) and aged device C (dotted black) for 2000 h at ambient light and temperature. Measured under 100 mW cm^{-2} simulated AM1.5 spectrum with an active area = 0.126 cm^2 .

$\eta = 5.20$ to 4.50% after aging of the cell, where this decrease was mainly caused by the deterioration of the FF from 0.58 to 0.53, with a slight decrease in V_{oc} from 580 to 569 mV and J_{sc} from 15.4 to 15.0 mA cm^{-2} . It is worth to mention here, that to our knowledge our EL1 redox system is one of the most stable thiolate/disulfide electrolyte used in a DSSC.^{40,75}

CONCLUSION

In conclusion, the use of the organic-based electrolyte (S^-/DS) in a DSSC has shown promising results when used with a MWCNT-COOH based CE with relatively very good long-term stability. The presented MWCNT-COOH CE was also investigated with the conventional iodide, thiolate and cobalt-based electrolyte systems, where it showed superior electrocatalytic activity with the latter two electrolyte systems and similar high catalytic activity toward the iodine-based electrolyte when compared to Pt. The good performance of the MWCNT-COOH CE was attributed to its high electroactive surface area and intrinsic electrocatalytic activity toward the regeneration of the four electrolyte systems investigated. This conclusion was arrived at by the means of performing voltammetry, Tafel plots and electrochemical impedance spectroscopy on fully functional DSSCs and dummy devices of the form CE//electrolyte//CE. R_{CT} values of $< 1 \Omega \text{ cm}^2$ at the MWCNT-COOH/electrolyte interface have been measured with the four different electrolyte systems. Further work is in progress to improve the conductivity properties of the MWCNT-COOH CE. This is being approached by incorporating graphene nanoplatelets into the films. In addition, we will be investigating the doping of the MWCNT-COOH films with other electroactive inorganic material by taking advantage of the high surface area of these films.

■ ASSOCIATED CONTENT

● Supporting Information

Synthetic scheme, D35 structure, and additional voltammetry spectra. This material is available free of charge via the Internet at <http://pubs.acs.org>.

■ AUTHOR INFORMATION

Corresponding Author

*E-mail: tarek.ghaddar@aub.edu.lb.

Notes

The authors declare no competing financial interest.

■ ACKNOWLEDGMENTS

This work was supported by the University Research Board (URB) at the American University of Beirut (AUB) and the Munib and Angela Masri Institute of Energy & Natural Resources (AUB).

■ REFERENCES

- (1) O'Regan, B.; Grätzel, M. A Low-Cost, High-Efficiency Solar Cell Based on Dye-Sensitized Colloidal TiO₂ Films. *Nature* **1991**, *353*, 737–740.
- (2) Yella, A.; Lee, H.-W.; Tsao, H. N.; Yi, C.; Chandiran, A. K.; Nazeeruddin, M. K.; Diao, E. W.-G.; Yeh, C.-Y.; Zakeeruddin, S. M.; Grätzel, M. Porphyrin-Sensitized Solar Cells with Cobalt (II/III) Based Redox Electrolyte Exceed 12% Efficiency. *Science* **2011**, *334*, 629–634.
- (3) Burschka, J.; Pellet, N.; Moon, S.-J.; Humphry-Baker, R.; Gao, P.; Nazeeruddin, M. K.; Grätzel, M. Sequential Deposition as a Route to High-Performance Perovskite-Sensitized Solar Cells. *Nature* **2013**, *499*, 316–319.
- (4) Chiba, Y.; Islam, A.; Watanabe, Y.; Komiya, R.; Koide, N.; Han, L. Dye-Sensitized Solar Cells with Conversion Efficiency of 11.1%. *Jpn. J. Appl. Phys.* **2006**, *45*, L638–L640.
- (5) Wang, M.; Grätzel, C.; Zakeeruddin, S. M.; Grätzel, M. Recent Developments in Redox Electrolytes for Dye-Sensitized Solar Cells. *Energy Environ. Sci.* **2012**, *5*, 9394–9405.
- (6) Cong, J.; Yang, X.; Kloo, L.; Sun, L. Iodine/Iodide-Free Redox Shuttles for Liquid Electrolyte-Based Dye-Sensitized Solar Cells. *Energy Environ. Sci.* **2012**, *5*, 9180–9194.
- (7) Teng, C.; Yang, X.; Yuan, C.; Li, C.; Chen, R.; Tian, H.; Li, S.; Hagfeldt, A.; Sun, L. Two Novel Carbazole Dyes for Dye-Sensitized Solar Cells with Open-Circuit Voltages up to 1 V Based on Br⁻/Br₃⁻ Electrolytes. *Org. Lett.* **2009**, *11*, 5542–5545.
- (8) Oskam, G.; Bergeron, B. V.; Meyer, G. J.; Searson, P. C. Pseudohalogens for Dye-Sensitized TiO₂ Photoelectrochemical Cells. *J. Phys. Chem. B* **2001**, *105*, 6867–6873.
- (9) Wang, P.; Zakeeruddin, S. M.; Moser, J.-E.; Humphry-Baker, R.; Grätzel, M. A Solvent-Free, SeCN⁻/(SeCN)₃⁻ Based Ionic Liquid Electrolyte Forhigh-Efficiency Dye-Sensitized Nanocrystalline Solar Cells. *J. Am. Chem. Soc.* **2004**, *126*, 7164–7165.
- (10) Daeneke, T.; Kwon, T. H.; Holmes, A. B.; Duffy, N. W.; Bach, U.; Spiccia, L. High-Efficiency Dye Sensitized Solar Cells with Ferrocene-Based Electrolytes. *Nat. Chem.* **2011**, *3*, 211–215.
- (11) Gregg, B. A.; Pichot, F.; Ferrere, S.; Fields, C. L. Interfacial Recombination Processes in Dye-Sensitized Solar Cells and Methods to Passivate the Interfaces. *J. Phys. Chem. B* **2001**, *105*, 1422–1429.
- (12) Hamann, T. W.; Farha, O. K.; Hupp, J. T. Performance Enhancement Based on Photoelectrode Modification via Atomic Layer Deposition. *J. Phys. Chem. C* **2008**, *112*, 19756–19764.
- (13) Caramori, S.; Husson, J.; Beley, M.; Bignozzi, C. A.; Argazzi, R.; Gros, P. C. Combination of Cobalt and Iron Polypyridine Complexes for Improving the Charge Separation and Collection in Ru-(terpyridine)₂-Sensitized Solar Cells. *Chem.—Eur. J.* **2010**, *16*, 2611–2618.
- (14) Hattori, S.; Wada, Y.; Yanagida, S.; Fukuzumi, S. Blue Copper Model Complexes with Distorted Tetragonal Geometry Acting as Effective Electron-Transfer Mediators in Dye-Sensitized Solar Cells. *J. Am. Chem. Soc.* **2005**, *127*, 9648–9654.
- (15) Li, T. C.; Spokoiny, A. M.; She, C.; Farha, O. K.; Mirkin, C. A.; Marks, T. J.; Hupp, J. T. Ni(III)/(IV) Bis(dicarbollide) as a Fast, Noncorrosive Redox Shuttle for Dye-Sensitized Solar Cells. *J. Am. Chem. Soc.* **2010**, *132*, 4580–4582.
- (16) Nusbaumer, H.; Zakeeruddin, S. M.; Moser, J. E.; Grätzel, M. An Alternative Efficient Redox Couple for the Dye-Sensitized Solar Cell System. *Chem.—Eur. J.* **2003**, *9*, 3756–3763.
- (17) Cazzanti, S.; Caramori, S.; Argazzi, R.; Elliott, C. M.; Bignozzi, C. A. Efficient Non-Corrosive Electron-Transfer Mediator Mixtures for Dye-Sensitized Solar Cells. *J. Am. Chem. Soc.* **2006**, *128*, 9996–9997.
- (18) Sapp, S. A.; Elliott, C. M.; Contado, C.; Caramori, S.; Bignozzi, C. A. Substituted Polypyridine Complexes of Cobalt(II/III) as Efficient Electron-Transfer Mediators in Dye-Sensitized Solar Cells. *J. Am. Chem. Soc.* **2002**, *124*, 11215–11222.
- (19) Klahr, B. M.; Hamann, T. W. Performance Enhancement and Limitations of Cobalt Bipyridyl Redox Shuttles in Dye-Sensitized Solar Cells. *J. Phys. Chem. C* **2009**, *113*, 14040–14045.
- (20) DeVries, M. J.; Pellin, M. J.; Hupp, J. T. Dye-Sensitized Solar Cells: Driving-Force Effects on Electron Recombination Dynamics with Cobalt Based Shuttles. *Langmuir* **2010**, *26*, 9082–9087.
- (21) Liu, Y.; Jennings, J. R.; Wang, Q. Efficient Dye-Sensitized Solar Cells Using a Tetramethylthiourea Redox Mediator. *ChemSusChem* **2013**, *6*, 2124–2131.
- (22) Noureldine, D.; Shoker, T.; Musameh, M.; Ghaddar, T. H. Investigation of Carbon Nanotube Webs as Counter Electrodes in a New Organic Electrolyte Based Dye Sensitized Solar Cell. *J. Mater. Chem.* **2012**, *22*, 862–869.
- (23) Cho, W.; Song, D.; Lee, Y.-G.; Chae, H.; Kim, Y. R.; Pyun, Y. B.; Nagarajan, S.; Sudhagar, P.; Kang, Y. S. Efficient Binary Organic Thiolate/Disulfide Redox Mediators in Dye-Sensitized Solar Cells Based on a Carbon Black Counter Electrode. *J. Mater. Chem. A* **2013**, *1*, 233–236.
- (24) Wang, M.; Chamberland, N.; Breau, L.; Moser, J.-E.; Humphry-Baker, R.; Marsan, B.; Zakeeruddin, S. M.; Grätzel, M. An Organic Redox Electrolyte to Rival Triiodide/Iodide in Dye-Sensitized Solar Cells. *Nat. Chem.* **2010**, *2*, 385–389.
- (25) Tian, H.; Jiang, X.; Yu, Z.; Kloo, L.; Hagfeldt, A.; Sun, L. Efficient Organic-Dye-Sensitized Solar Cells Based on an Iodine-Free Electrolyte. *Angew. Chem., Int. Ed.* **2010**, *49*, 7328–7331.
- (26) Tian, H.; Yu, Z.; Hagfeldt, A.; Kloo, L.; Sun, L. Organic Redox Couples and Organic Counter Electrode for Efficient Organic Dye-Sensitized Solar Cells. *J. Am. Chem. Soc.* **2011**, *133*, 9413–9422.
- (27) Tian, H.; Sun, L. Iodine-Free Redox Couples for Dye-Sensitized Solar Cells. *J. Mater. Chem.* **2011**, *21*, 10592–10601.
- (28) Liu, Y.; Jennings, J. R.; Parameswaran, M.; Wang, Q. An Organic Redox Mediator for Dye-Sensitized Solar Cells with near Unity Quantum Efficiency. *Energy Environ. Sci.* **2011**, *4*, 564–571.
- (29) Li, X.; Ku, Z.; Rong, Y.; Liu, G.; Liu, L.; Liu, T.; Hu, M.; Yang, Y.; Wang, H.; Xu, M.; Xiang, P.; Han, H. Design of an Organic Redox Mediator and Optimization of an Organic Counter Electrode for Efficient Transparent Bifacial Dye-Sensitized Solar Cells. *Phys. Chem. Chem. Phys.* **2012**, *14*, 14383–14390.
- (30) Li, X.; Liu, L.; Liu, G.; Rong, Y.; Yang, Y.; Wang, H.; Ku, Z.; Xu, M.; Zhong, C.; Han, H. Efficient Dye-Sensitized Solar Cells with Potential-Tunable Organic Sulfide Mediators and Graphene-Modified Carbon Counter Electrodes. *Adv. Funct. Mater.* **2013**, *23*, 3344–3352.
- (31) Li, D.; Li, H.; Luo, Y.; Li, K.; Meng, Q.; Armand, M.; Chen, L. Non-Corrosive, Non-Absorbing Organic Redox Couple for Dye-Sensitized Solar Cells. *Adv. Funct. Mater.* **2010**, *20*, 3358–3365.
- (32) Guo, W.; Shen, Y.; Wu, M.; Wang, L.; Wang, L.; Ma, T. SnS-Quantum Dot Solar Cells Using Novel TiC Counter Electrode and Organic Redox Couples. *Chem.—Eur. J.* **2012**, *18*, 7862–7868.

- (33) Ning, Z.; Tian, H.; Yuan, C.; Fu, Y.; Sun, L.; Ågren, H. Pure Organic Redox Couple for Quantum-Dot-Sensitized Solar Cells. *Chem.—Eur. J.* **2011**, *17*, 6330–6333.
- (34) Xu, X.; Zhang, B.; Cui, J.; Xiong, D.; Shen, Y.; Chen, W.; Sun, L.; Cheng, Y.; Wang, M. Efficient p-Type Dye-Sensitized Solar Cells Based on Disulfide/Thiolate Electrolytes. *Nanoscale* **2013**, *5*, 7963–7969.
- (35) Ahmad, S.; Yum, J.-H.; Butt, H.-J.; Nazeeruddin, M. K.; Grätzel, M. Efficient Platinum-Free Counter Electrodes for Dye-Sensitized Solar Cell Applications. *ChemPhysChem* **2010**, *11*, 2814–2819.
- (36) Syrokostas, G.; Siokoub, A.; Leftheriotis, G.; Yianoulis, P. Degradation Mechanisms of Pt Counter Electrodes for Dye Sensitized Solar Cells. *Sol. Energy Mater. Sol. C* **2012**, *103*, 119–127.
- (37) Wang, L.; Wu, M.; Gao, Y.; Ma, T. Highly Catalytic Counter Electrodes for Organic Redox Couple of Thiolate/Disulfide in Dye-Sensitized Solar Cells. *Appl. Phys. Lett.* **2011**, *98*, 221101–221103.
- (38) Wu, M.; Bai, J.; Wang, Y.; Wang, A.; Lin, X.; Wang, L.; Shen, Y.; Wang, Z.; Hagfeldt, A.; Ma, T. High-Performance Phosphide/Carbon Counter Electrode for Both Iodide and Organic Redox Couples in Dye-Sensitized Solar Cells. *J. Mater. Chem.* **2012**, *22*, 11121–11127.
- (39) Tian, H.; Gabrielson, E.; Yu, Z.; Hagfeldt, A.; Kloo, L.; Sun, L. A Thiolate/Disulfide Ionic Liquid Electrolyte for Organic Dye-Sensitized Solar Cells Based on Pt-Free Counter Electrodes. *Chem. Commun.* **2011**, *47*, 10124–10126.
- (40) Burschka, J.; Brault, V.; Ahmad, S.; Breau, L.; Nazeeruddin, M. K.; Marsan, B.; Zakeeruddin, S. M.; Grätzel, M. Influence of the Counter Electrode on the Photovoltaic Performance of Dye-Sensitized Solar Cells Using a Disulfide/Thiolate Redox Electrolyte. *Energy Environ. Sci.* **2012**, *5*, 6089–6097.
- (41) Ku, Z.; Li, X.; Liu, G.; Wang, H.; Rong, Y.; Xu, M.; Liu, L.; Hu, M.; Yang, Y.; Han, H. Transparent NiS Counter Electrodes for Thiolate/Disulfide Mediated Dye-Sensitized Solar Cells. *J. Mater. Chem. A* **2013**, *1*, 237–240.
- (42) Liu, G.; Li, X.; Wang, H.; Rong, Y.; Ku, Z.; Xu, M.; Liu, L.; Hu, M.; Yang, Y.; Han, H. An Efficient Thiolate/Disulfide Redox Couple Based Dye-Sensitized Solar Cell with a Graphene Modified Mesoscopic Carbon Counter Electrode. *Carbon* **2012**, *53*, 11–18.
- (43) Zhang, J.; Long, H.; Miralles, S. G.; Bisquert, J.; Fabregat-Santiago, F.; Zhang, M. The Combination of a Polymer-Carbon Composite Electrode with a High-Absorptivity Ruthenium Dye Achieves an Efficient Dye-Sensitized Solar Cell Based on a Thiolate-Disulfide Redox Couple. *Phys. Chem. Chem. Phys.* **2012**, *14*, 7131–7136.
- (44) Wu, H.; Lv, Z.; Chu, Z.; Wang, D.; Hou, S.; Zou, D. Graphite and Platinum's Catalytic Selectivity for Disulfide/Thiolate (T_2/T^-) and Triiodide/Iodide (I_3^-/I^-). *J. Mater. Chem.* **2011**, *21*, 14815–14820.
- (45) Pan, S.; Yang, Z.; Li, H.; Qiu, L.; Sun, H.; Peng, H. Efficient Dye-Sensitized Photovoltaic Wires Based on an Organic Redox Electrolyte. *J. Am. Chem. Soc.* **2013**, *135*, 10622–10625.
- (46) Hao, F.; Dong, P.; Zhang, J.; Zhang, Y.; Loya, P. E.; Hauge, R. H.; Li, J.; Lou, J.; Lin, H. High Electrocatalytic Activity of Vertically Aligned Single-Walled Carbon Nanotubes Towards Sulfide Redox Shuttles. *Sci. Rep.* **2012**, *2*, srep00368.
- (47) Hao, F.; Wang, Z.; Luo, Q.; Lou, J.; Li, J.; Wang, J.; Fan, S.; Jiang, K.; Lin, H. Highly Catalytic Cross-Stacked Superaligned Carbon Nanotube Sheets for Iodine-Free Dye-Sensitized Solar Cells. *J. Mater. Chem.* **2012**, *22*, 22756–22762.
- (48) Salvatori, P.; Marotta, G.; Cinti, A.; Anselmi, C.; Mosconi, E.; De Angelis, F. Supramolecular Interactions of Chenodeoxycholic Acid Increase the Efficiency of Dye-Sensitized Solar Cells Based on a Cobalt Electrolyte. *J. Phys. Chem. C* **2013**, *117*, 3874–3887.
- (49) O'Regan, B. C.; Durrant, J. R.; Sommeling, P. M.; Bakker, N. J. Influence of the $TiCl_4$ Treatment on Nanocrystalline TiO_2 Films in Dye-Sensitized Solar Cells. 2. Charge Density, Band Edge Shifts, and Quantification of Recombination Losses at Short Circuit. *J. Phys. Chem. C* **2007**, *111*, 14001–14010.
- (50) Datta, J.; Bhattacharya, A.; Kundu, K. K. Relative Standard Electrode Potentials of Triiodide/Iodide, Iodine/Triiodide and Iodine/Iodide Redox Couples and the Related Formation Constants of I_3^- in Some Pure and Mixed Dipolar Aprotic Solvents. *Bull. Chem. Soc. Jpn.* **1988**, *61*, 1735–1742.
- (51) Roy-Mayhew, J. D.; Bozym, D. J.; Punckt, C.; Aksay, I. A. Functionalized Graphene as a Catalytic Counter Electrode in Dye-Sensitized Solar Cells. *ACS Nano* **2010**, *4*, 6203–6211.
- (52) Park, B.-w.; Pazoki, M.; Aitola, K.; Jeong, S.; Johansson, E. M. J.; Hagfeldt, A.; Boschloo, G. Understanding Interfacial Charge Transfer between Metallic PEDOT Counter Electrodes and a Cobalt Redox Shuttle in Dye-Sensitized Solar Cells. *ACS Appl. Mater. Interfaces* **2014**, *6*, 2074–2079.
- (53) Kavan, L.; Yum, J.-H.; Nazeeruddin, M. K.; Grätzel, M. Graphene Nanoplatelet Cathode for Co(III)/(II) Mediated Dye-Sensitized Solar Cells. *ACS Nano* **2011**, *5*, 9171–9178.
- (54) Hauch, A.; Georg, A. Diffusion in the Electrolyte and Charge-Transfer Reaction at the Platinum Electrode in Dye-Sensitized Solar Cells. *Electrochim. Acta* **2001**, *46*, 3457–3466.
- (55) Lee, K. S.; Lee, W. J.; Park, N.-G.; Kim, S. O.; Park, J. H. Transferred Vertically Aligned N-doped Carbon Nanotube Arrays: Use in Dye-Sensitized Solar Cells as Counter Electrodes. *Chem. Commun.* **2011**, *47*, 4264–4266.
- (56) Dong, P.; Pint, C. L.; Hainey, M.; Mirri, F.; Zhan, Y.-J.; Zhang, J.; Pasquali, M.; Hauge, R. H.; Verduzco, R.; Jiang, M.; Lin, H.; Lou, J. Vertically Aligned Single-Walled Carbon Nanotubes as Low-Cost and High Electrocatalytic Counter Electrode for Dye-Sensitized Solar Cells. *ACS Appl. Mater. Interfaces* **2011**, *3*, 3157–3161.
- (57) Yang, Z.; Chen, T.; He, R.; Guan, G.; Li, H.; Qiu, L.; Peng, H. Aligned Carbon Nanotube Sheets for the Electrodes of Organic Solar Cells. *Adv. Mater.* **2011**, *23*, 5436–5439.
- (58) Chen, J.; Meng, F.; Gui, X.; Sun, H.; Zeng, Z.; Li, Z.; Zhou, Y.; Tang, Z. The Application of a Three Dimensional CNT-Sponge as the Counter Electrode for Dye-Sensitized Solar Cells. *Carbon* **2012**, *50*, 5624–5627.
- (59) Jo, Y.; Cheon, J. Y.; Yu, J.; Jeong, H. Y.; Han, C.-H.; Jun, Y.; Joo, S. H. Highly Interconnected Ordered Mesoporous Carbon-Carbon Nanotube Nanocomposites: Pt-Free, Highly Efficient, and Durable Counter Electrodes for Dye-Sensitized Solar Cells. *Chem. Commun.* **2012**, *48*, 8057–8059.
- (60) Han, J.; Kim, H.; Kim, D. Y.; Jo, S. M.; Jang, S.-Y. Water-Soluble Polyelectrolyte-Grafted Multiwalled Carbon Nanotube Thin Films for Efficient Counter Electrode of Dye-Sensitized Solar Cells. *ACS Nano* **2010**, *4*, 3503–3509.
- (61) Wu, M.; Lin, X.; Wang, T.; Qiu, J.; Ma, T. Low-Cost Dye-Sensitized Solar Cell Based on Nine Kinds of Carbon Counter Electrodes. *Energy Environ. Sci.* **2011**, *4*, 2308–2315.
- (62) Choi, H. J.; Gong, H. H.; Park, J.-Y.; Hong, S. C. Characteristics of Dye-Sensitized Solar Cells with Surface-Modified Multi-Walled Carbon Nanotubes as Counter Electrodes. *J. Mater. Sci.* **2013**, *48*, 906–912.
- (63) Munkhbayar, B.; Hwang, S.; Kim, J.; Bae, K.; Ji, M.; Chung, H.; Jeong, H. Photovoltaic Performance of Dye-Sensitized Solar Cells with Various MWCNT Counter Electrode Structures Produced by Different Coating Methods. *Electrochim. Acta* **2012**, *80*, 100–107.
- (64) Chen, Y.; Zhang, H.; Chen, Y.; Lin, J. Study on Carbon Nanocomposite Counterelectrode for Dye-Sensitized Solar Cells. *J. Nanomater.* **2012**, 601736.
- (65) Balamurugan, J.; Thangamuthu, R.; Pandurangan, A. Growth of Carbon Nanotubes over Transition Metal Loaded on Co-Sb₂S₃ and Its Application for High Performance Dye-Sensitized Solar Cells. *J. Mater. Chem. A* **2013**, *1*, 5070–5080.
- (66) Malara, F.; Manca, M.; De Marco, L.; Pareo, P.; Gigli, G. Flexible Carbon Nanotube-Based Composite Plates as Efficient Monolithic Counter Electrodes for Dye Solar Cells. *ACS Appl. Mater. Interfaces* **2011**, *3*, 3625–3632.
- (67) Wang, Q.; Ito, S.; Grätzel, M.; Fabregat-Santiago, F.; Mora-Seró, I. n.; Bisquert, J.; Bessho, T.; Imai, H. Characteristics of High Efficiency Dye-Sensitized Solar Cells. *J. Phys. Chem. B* **2006**, *110*, 25210–25221.

(68) Fabregat-Santiago, F.; Garcia-Belmonte, G.; Mora-Sero, I.; Bisquert, J. Characterization of Nanostructured Hybrid and Organic Solar Cells by Impedance Spectroscopy. *Phys. Chem. Chem. Phys.* **2011**, *13*, 9083–9118.

(69) Bisquert, J. Chemical Capacitance of Nanostructured Semiconductors: Its Origin and Significance for Nanocomposite Solar Cells. *Phys. Chem. Chem. Phys.* **2003**, *5*, 5360–5364.

(70) González-Pedro, V.; Xu, X.; Mora-Seró, I. N.; Bisquert, J. Modeling High-Efficiency Quantum Dot Sensitized Solar Cells. *ACS Nano* **2010**, *4*, 5783–5790.

(71) Guillén, E.; Peter, L. M.; Anta, J. A. Electron Transport and Recombination in ZnO-Based Dye-Sensitized Solar Cells. *J. Phys. Chem. C* **2011**, *115*, 22622–22632.

(72) Boschloo, G.; Hagfeldt, A. Characteristics of the Iodide/Triiodide Redox Mediator in Dye-Sensitized Solar Cells. *Acc. Chem. Res.* **2009**, *42*, 1819–1826.

(73) Bard, A.; Faulkner, L. *Electrochemical Methods, Fundamentals and Applications*, 2nd ed.; Wiley: New York, 2001.

(74) Cañete-Rosales, P.; Ortega, V.; Álvarez-Lueje, A.; Bollo, S.; González, M.; Ansón, A.; Martínez, M. T. Influence of Size and Oxidative Treatments of Multi-Walled Carbon Nanotubes on Their Electrocatalytic Properties. *Electrochim. Acta* **2012**, *62*, 163–171.

(75) Liu, L.; Li, X.; Chen, J.; Rong, Y.; Ku, Z.; Han, H. Improvement of Thiolate/Disulfide Mediated Dye-Sensitized Solar Cells through Supramolecular Lithium Cation Assembling of Crown Ether. *Sci. Rep.* **2013**, *3*, 1–5.